A Numerical Analysis of Shaft Stress Concentration Using ANSYS

Abdul Wahhab N. Abbas
Department of Mechanics, Anbar Technical Institute, Middle Technical University, Anbar, Iraq
wahabani@mtu.edu.iq

Ahmed Hussein
Department of Mechanics, Anbar Technical Institute, Middle Technical University, Anbar, Iraq
ahmedhussein@mtu.edu.iq

Hasan A. Al Shubber
Department of Mechanical Engineering, College of Engineering, Baghdad University, Baghdad, Iraq
h.al-shubber1303@coeng.uobaghdad.edu.iq (corresponding author)

Received: 24 March 2025 | Revised: 15 April 2025, 27 April 2025, 13 May 2025, 28 May 2025, and 15 June 2025 | Accepted: 3 July 2025

 DOI: https://doi.org/10.48084/etasr.11111

ABSTRACT

Stress Concentration (SC) in shafts is a critical factor leading to deformation and failure, particularly in power transmission systems. This study investigates Stress Concentration Factors (SCFs) for three shaft geometries—shoulder fillet, chamfer, and key-seat—under tension, torsion, and bending loads using Finite Element Analysis (FEA) in ANSYS 2023 R2. The numerical results revealed significant variations in SCFs across the geometries and load types. Under tension, the chamfered shaft exhibited the highest SCF (2.967), while the shoulder fillet (1.645) and key-seat (1.603) showed comparable values. Torsion loading maximized the SCFs in the key-seat (2.413), whereas bending produced nearly identical SCFs for the chamfer (2.512) and key-seat (2.503). Validations against previous studies confirmed the accuracy of the FEA approach. The findings highlight that the shoulder fillets consistently minimize the SC, while chamfers, despite the higher SCFs, offer cost-effective manufacturability.

Keywords-stress concentration; shaft; deformation; numerical analysis; shoulder fillet

I. INTRODUCTION

Shafts are integral components in mechanical systems used for power and torque transmission in applications, such as automotive gearboxes, turbines, and electric motors. However, the presence of geometric discontinuities, such as shoulders, key-seats, and chamfers introduces a localized increase in stress known as SC. These SCs reduce the fatigue strength of the shaft and are often the root cause of mechanical failure under cyclic or combined loading conditions [1].

SCFs quantify the amplification of stress at geometric irregularities relative to nominal stress, making them an essential design consideration. The accurate determination of SCF is vital to improving the shaft performance, increasing the operational life, and preventing catastrophic failures. Although analytical methods based on empirical formulas provide initial estimates, their applicability is limited to simplified geometries and idealized loading conditions. In contrast, the Finite Element Method (FEM) enables the precise modeling of complex geometries under realistic boundary and loading conditions and has become the preferred tool for such analyses [2-4].

The FEM studies have focused on key-seat and shoulder fillet designs, examining the influence of parameters, such as fillet radius, taper angle, and key-seat dimensions. Authors in [5] combined analytical and numerical methods to determine the optimal shaft diameters in the presence of key-seats, revealing the trade-off between the weight and stress reduction. In [6], a novel elliptical key design achieved a stress reduction of 78%, enhancing the fatigue resistance. Other studies explored the effect of the key-seat geometry under torsional [7], bending [8], and combined loadings [9], indicating the significant influence of small changes in dimension or curvature on SCFs. Recent developments have also included optimization-based approaches. For instance, the numerical shape optimization in [10] resulted in SCF reductions of up to 49%, while material selection strategies have been also integrated to further enhance performance [11, 12]. Authors in [13] investigated the taper and shoulder transitions, demonstrating SCF variations based on the load type and geometry transition angle. Authors in [14], though, focused on the determination of the shaft SCF under tension only. However, most of these works either focus on a single loading condition or fail to cross-validate the numerical results with established analytical formulas and prior FEM benchmarks

[15-21]. Additionally, research has overlooked the mesh convergence studies, solver configurations, or boundary condition specifications—elements essential for the numerical accuracy.

There is also a limited number of studies that evaluate the SCFs for multiple shaft features—shoulders, chamfers, and keyways—under various loading scenarios (tension, torsion, and bending) in a unified framework. The need for such a comparative and validated study is evident, especially in high-stake applications, where shaft failure leads to major operational losses.

To address these gaps, the current study presents a validated finite element investigation of SCFs in shafts featuring three typical geometrical discontinuities: shoulder fillets, chamfers, and key-seats. Each case is analyzed under three common loading types using ANSYS Workbench 2023 R2. The mesh sensitivity is tested, and the results are validated against analytical expressions from [1] and FEM benchmarks from [7]. This integrated approach not only highlights the most vulnerable configurations, but also informs the practical shaft design in automotive, aerospace, and industrial systems. The study aligns with the findings in [21], emphasizing the numerical rigor and application-focused analysis.

II. METHODOLOGY

A. Studied Cases

The SC in shafts can be induced by different factors, such as shoulders, diameter change, key-seats, etc. Three main cases were analyzed. The first one is a stepped shaft with a shoulder fillet, the second is replacing the fillet with a chamfer, and the third is a shaft with a key-seat. The SCF was investigated under different loadings and a parametric study was employed regarding the design parameters for each case:

- Shoulder Fillet: a 50 mm small diameter stepped shaft was presented in this work, while the larger diameter is 70 mm, and the fillet radius is 10 mm.
- Chamfers: they have similar parameters to case 1, except for the chamfer height and width, which are 10 mm and 6 mm, respectively.
- Shaft key-seat: a 50 mm diameter shaft with key-seat height and width of 6.25 mm and 12.5 mm, respectively, while the radius of the fillet is 3.5 mm based on [1].

B. Governing Equations

The governing equations of this analysis are:

- The SCF of the stepped shafts with shoulder fillets under tensile load can be calculated as [1]:

$$K_t = \frac{\sigma_{\max}}{\sigma_{\text{nom}}} \quad (1)$$

$$\sigma_{\text{nom}} = \frac{4\,P}{\pi d^2} \quad (2)$$

where K_t is the tensile SCF, σ_{max} is the maximum tensile stress at the shoulder (MPa), σ_{nom} is the nominal tensile stress in the shaft (MPa), P is the axial applied load (N), and d is the smallest shaft diameter (mm).

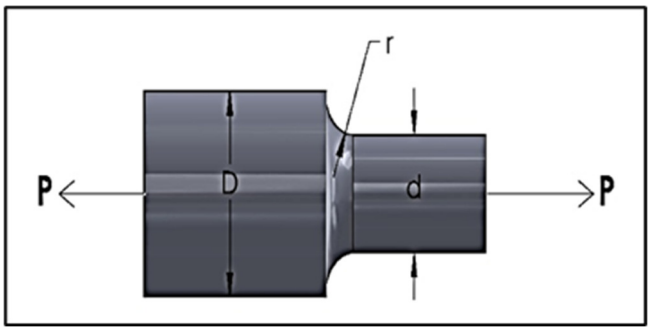

Fig. 1. Design parameters for case 1 under tensile load.

$$K_{ts} = \frac{\tau_{\max}}{\tau_{\text{nom}}} \quad (3)$$

$$\tau_{\text{nom}} = \frac{16\,T}{\pi d^3} \quad (4)$$

where K_{ts} is the torsional SCF, τ_{max} is the maximum shear stress at the shoulder (MPa), τ_{nom} is the nominal shear stress in the shaft (MPa), and T is the applied torsional torque (Nm).

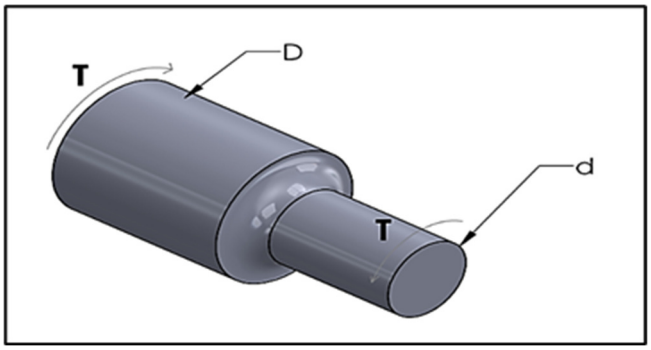

Fig. 2. Design parameters for case 1 under torsional loading.

- Under bending load as in Figure 3 [1]:

$$K_{tb} = \frac{\sigma_{\max}}{\sigma_{\text{nom}}} \quad (5)$$

$$\sigma_{\text{nom}} = \frac{32\,M}{\pi d^3} \quad (6)$$

where K_{tb} is the bending SCF, σ_{max} is the maximum bending stress at the shoulder (MPa), σ_{nom} is the nominal bending stress in the shaft (MPa), and M is the applied moment (Nm).

- As for the stepped shafts with chamfer, the same above equations are applied. A comparison between the shoulder and chamfer configurations will be presented.
- Regarding the shafts with a key-seat, (5) and (6) are applied to all loadings, and the design parameters are shown in Figure 4.

C. Numerical Analysis

The numerical analysis was conducted using ANSYS 2023 R2 Workbench [22], where the geometry was sketched for each case by the design modular tool and the main diameter of the shaft (d = 50 mm) was fixed.

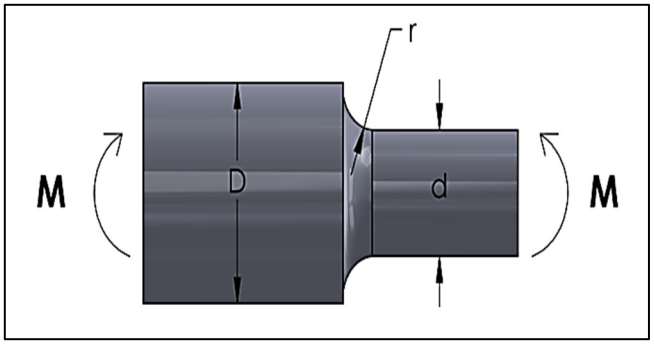

Fig. 3. Design parameters for case 2 under bending load.

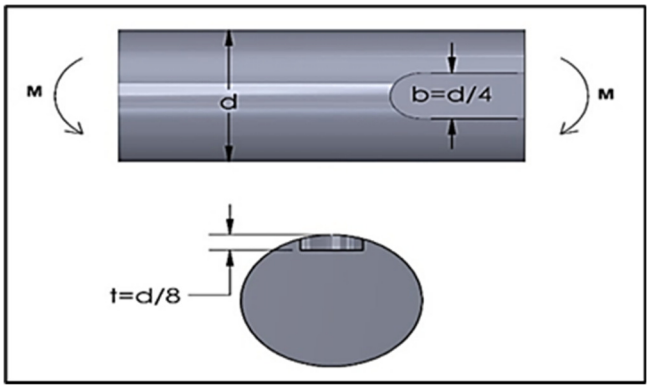

Fig. 4. A shaft with a key-seat under bending.

The mesh size was 2 mm for cases 1 and 2, while the mesh size for case 3 was 1 mm, as depicted in Figure 5. The boundary conditions used in this analysis are presented similarly to the cases above with hexahedral elements, where a tension force of 500 N was applied on the front face of the shaft, and a fixed support on the back face of the shaft, as portrayed in Figure 6 (a). The torsional moment was also applied on the front face of the shaft, as seen in Figure 6 (b), where the torsional moment was 50 Nm. Similarly, the bending moment of 50 Nm was applied as the other loadings, and the fixed support was attached to the other shaft face, as illustrated in Figure 6 (c).

A mesh convergence test was employed to check the mesh sensitivity of the results, and the error percentage was 0.2344 % in the worst expected case, as shown in Figure 7. The test took 804488 nodes and 576234 elements for the first round to analyze the results, while the second round utilized 1607950 nodes and 1159204 elements, without any significant changes in stresses. The analysis was performed using static structural settings, focusing on the Von Mises stress evaluation and employing an iterative solver.

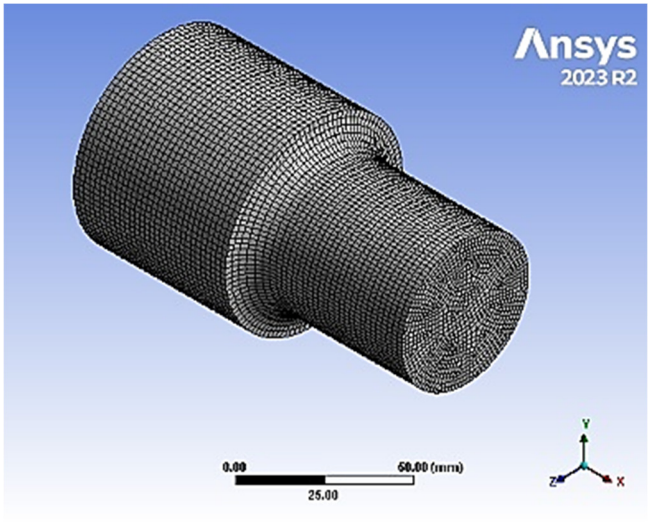

Fig. 5. Mesh size.

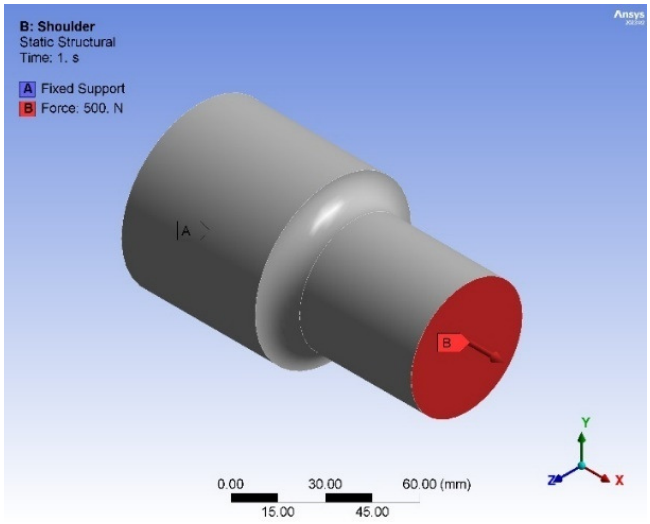

(a)

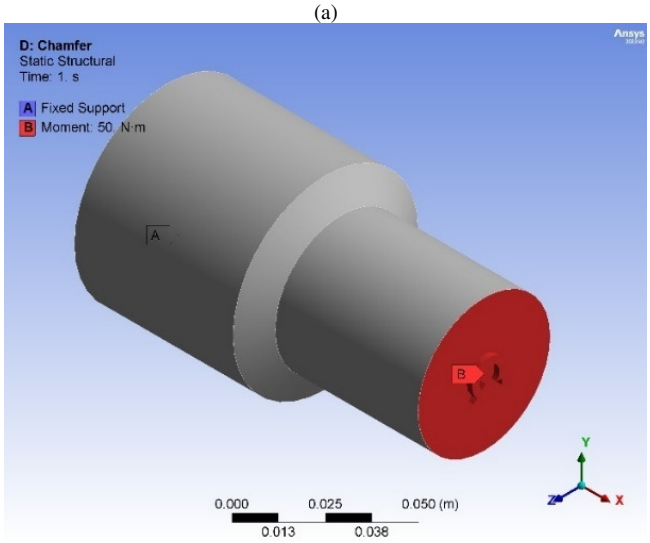

(b)

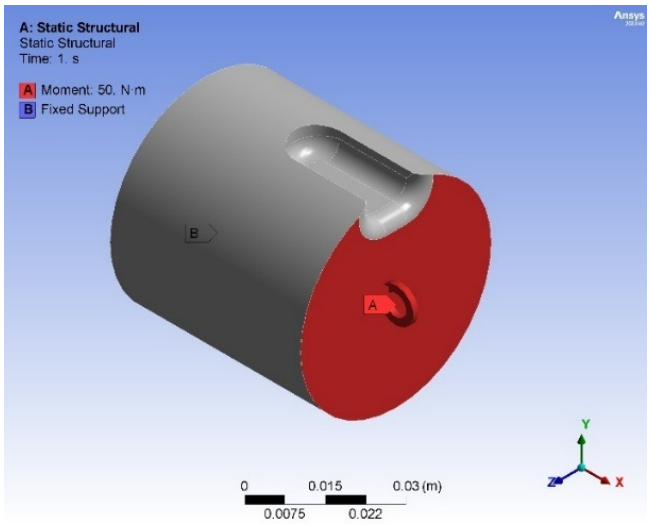

(c)

Fig. 6. The boundary conditions for: (a) tension force, (b) torsional moment, (c) banding moment.

III. RESULTS AND DISCUSSION

The results of this analysis for the three cases under three loading types are presented as follows:

A. Results Validation

The FEA results were validated against the findings in [1, 23] as displayed in Figure 8. A good agreement was achieved with an error percentage of 2 % in the SCF with the torsional load, and when r/d = 0.2, as shown in Table I. Another validation was performed against the findings in [7], as presented in Figure 9, where the error percentage was 1.65 %, as evidenced in Table I.

B. Tension Results

The FEA tension results of the shoulder fillet case are seen in Figure 10, where, as expected, the maximum stress (0.419 MPa) occurred at the fillet area when the tension force was 500 N, as shown in Figure 6 (a). The FEA nominal stress was 0.25465 MPa, while the nominal stress of this case based on (2) was 0.2547 MPa. Table II outlines the results of the SCF for the shoulder fillet case and the error percentage between the analytical and numerical nominal stress results, where the error percentage was 0.0196 % and the SCF was 1.645.

The FEA tension results of the chamfer case are shown in Figure 11 (a), where the maximum stress (0.75565 MPa) occurred at the chamfer area when the tension force was 500 N, as depicted in Figure 6 (a), and the FEA nominal stress was 0.25465 MPa, while the nominal stress of this case based on (2) was 0.2547 MPa. It is observed that the same error percentage for the nominal stress occurred, while the SCF for this case was 2.967, as seen in Table II.

Figure 11 (b) illustrates the FEA tension results for the shaft key-seat case, where the maximum stress (0.40836 MPa) occurred at the key-seat area when the tension force was 500 N, as displayed in Figure 6 (a), and the FEA nominal stress was 0.25465 MPa, as presented in Figure 10 (a), while the nominal stress of this case based on (2) was 0.2547 MPa.

It is noted that the same error percentage for the nominal stress occurred, while the SCF for this case was 1.603, as seen in Table II. The tension results showed that using chamfer in stepped shafts increases the SCF compared to the use of shoulder fillets, but the production of chamfer is better due its ease and cost. Regarding the SCF of the shaft key-seat, the results showed that the key-seated shafts had lower SC than the stepped shafts.

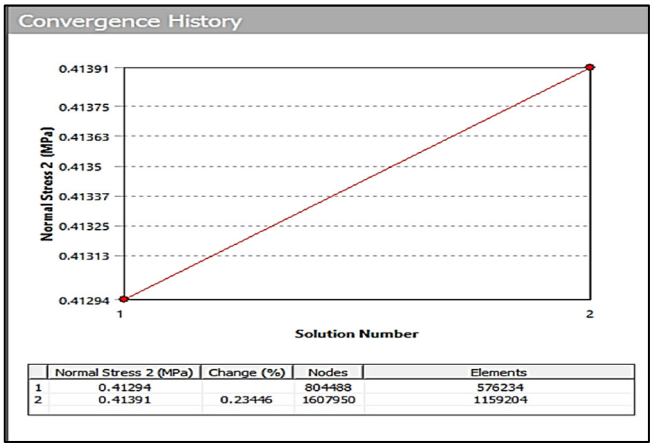

Fig. 7. Convergence test curve.

TABLE I. ERROR PERCENTAGE FOR BOTH VALIDATIONS

Type of stress	FEA result	Reference	Error %
Validation 1: K_{ts} [1, 23]	1.1270	1.1500	2.00
Validation 2: Von-Mises stress (MPa) [7]	36.085	36.691	1.65

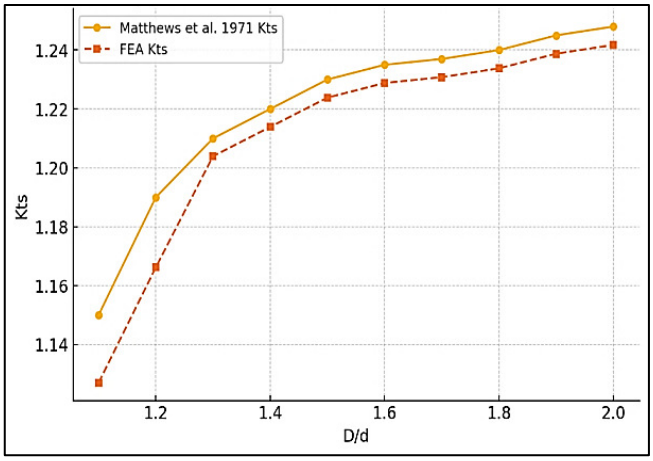

Fig. 8. Validation of the numerical results with [1, 23].

C. Torsion Results

The FEA torsion results of the shoulder fillet case are presented in Figure 12, where, as expected, the maximum stress (2.4396 MPa) occurred at the fillet area when the torque was 50 Nm, as illustrated in Figure 6 (b). The FEA nominal stress was 2.0377 MPa, while the nominal stress of this case based on (4) was 2.038 MPa. The SCF for the shoulder fillet case and the error percentage between the analytical and

numerical nominal stress results are shown in Table III, where the error percentage was 0.0147 % and the SCF 1.197.

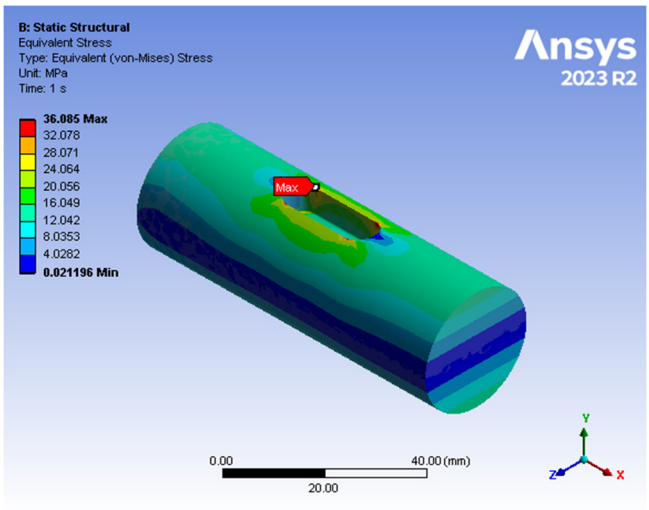

Fig. 9. FEA validated Von-Mises stress.

Figure 13 (a) presents the FEA torsion results for the second case, where the maximum shear stress (3.5556 MPa) occurred at the chamfer area when the tension force was 500 N, as shown in Figure 6 (b), and the FEA nominal stress was 2.0377 MPa, while the nominal stress of this case based on (4) was 2.038 MPa. The same error percentage for the nominal shear stress occurred, while the SCF for this case was 1.745, as seen in Table III. The FEA torsion results of the key-seat case are depicted in Figure 13 (b), where the maximum shear stress (4.9167 MPa) occurred at the key-seat when the torque was 50 Nm, as illustrated in Figure 6 (b), and the FEA nominal shear stress was 2.0377 MPa, while the nominal shear stress of this case based on (4) was 2.038 MPa. The key-seat's higher SCF (2.413) under torsion arises from abrupt geometric discontinuities, intensifying the shear SC compared to the fillets' smooth transitions. The SCF for the key-seat case and the error percentage between the analytical and numerical nominal stress results are portrayed in Table III, where the error percentage was 0.0147 % and the SCF 2.413.

TABLE II. TENSION SCF AND ERROR PERCENTAGE BETWEEN ANALYTICAL AND NUMERICAL NOMINAL STRESS

Case	1	2	3
Analytical nominal stress (MPa)	0.2547	0.2547	0.2547
FEA nominal stress (MPa)	0.2546	0.2546	0.2546
Error (%)	0.0196	0.0196	0.0196
FEA maximum shear stress (MPa)	0.4190	0.7556	0. 4083
SCF K_t	1.6450	2.9670	1.6030

The findings of the FEA under torsional loads revealed that the maximum SC occurred in the key-seat case, unlike for the tension loads. It is also clear that the shoulder fillet case is lower than the chamfer case in terms of the torsional loads.

D. Bending Results

The FEA bending results for the shoulder fillet case are exhibited in Figure 14, where, as expected, the maximum stress (5.8077 MPa) occurred at the fillet area when the bending moment was 50 Nm, as shown in Figure 6 (c), and the FEA nominal stress was 4.0743 MPa, while the nominal stress of this case based on (6) was 4.0764 MPa. Figure 15 (a) demonstrates the FEA bending results for the second case (stepped shaft with chamfer), where the maximum stress (10.239 MPa) occurred at the chamfer area, with the same bending stress. The FEA bending stress for the key-seat case is shown in Figure 15 (b), where the maximum stress (10.203 MPa) occurred at the key-seat area.

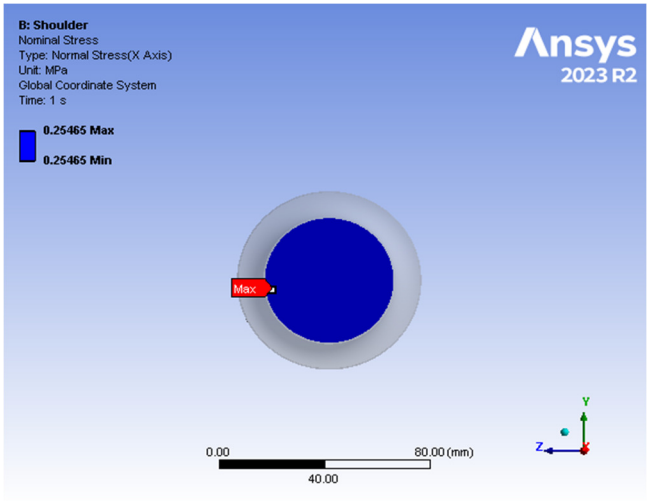

(a)

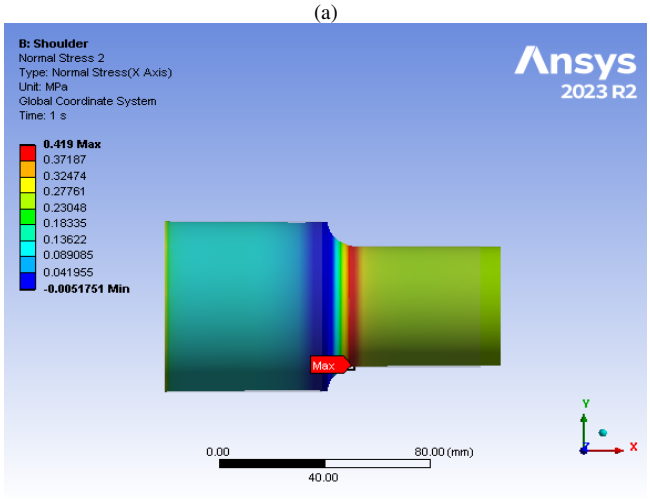

(b)

Fig. 10. FEA results for case 1: (a) nominal stress, (b) maximum stress.

TABLE III. TORSION SCF AND ERROR PERCENTAGE BETWEEN ANALYTICAL AND NUMERICAL NOMINAL SHEAR STRESS

Case	1	2	3
Analytical nominal stress (MPa)	2.038	2.038	2.038
FEA nominal stress (MPa)	2.037	2.037	2.037
Error (%)	0.0147	0.0147	0.0147
FEA maximum shear stress (MPa)	2.4396	3.556	4.917
SCF K_{ts}	1.197	1.745	2.413

The SCF results for the three cases under bending are presented in Table IV, where the error percentage was 0.0515%, and the SCF values were 1.425, 2.512, and 2.503 for the three cases, respectively. The tension and bending revealed similar SCFs for the key-seats and chamfers, while the fillets consistently minimized the SC. Torsion uniquely maximized the SCFs in key-seats due to the shear localization.

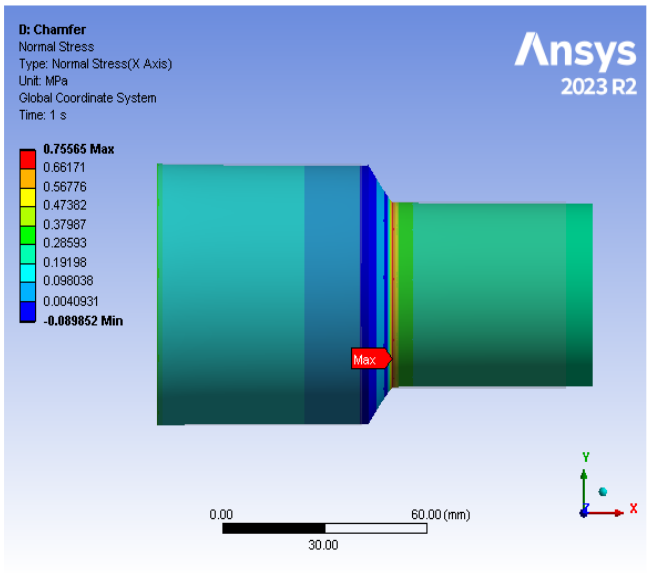

(a)

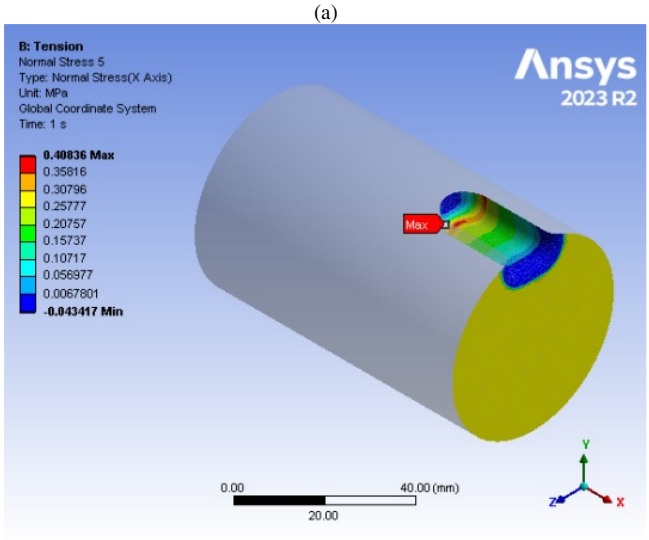

(b)

Fig. 11. FEA maximum stress: (a) case 2, (b) case 3.

The comparative analysis revealed distinct SCF trends for the shoulder fillets, chamfers, and key-seats under tension, torsion, and bending. Under tension, the chamfers exhibited the highest SCF (2.967), nearly doubling the values for the shoulder fillets (1.645) and key-seats (1.603), attributed to sharp geometric transitions amplifying the axial stress. In torsion, the key-seats recorded the worst performance (SCF = 2.413) due to abrupt discontinuities intensifying the shear stress, while the chamfers (1.745) and fillets (1.197) showed moderate and minimal concentrations, respectively. For bending, the chamfers (2.512) and key-seats (2.503) produced nearly identical SCFs, reflecting similar bending stress localization, whereas fillets (1.425) again demonstrated superior stress distribution. Across all load types, the shoulder fillets consistently minimized SCFs, validating their efficacy in critical applications. Chamfers, despite the higher SCFs, remained viable for cost-sensitive designs, while the key-seats required careful optimization under torsional loads to mitigate failure risks. This interplay underscores the necessity of geometry-specific load considerations in shaft design.

E. Result Comparison

Table V provides a comparison of the SCFs across all forms studied and different load conditions, offering an integrated overview of the relative performance of each design. The shoulder fillet was used as the baseline for comparison, as it consistently demonstrated superior performance, and the percentage increases were calculated relative to it. A comprehensive analysis of the SC coefficients shows shoulder fillet superiority in most load situations, achieving the lowest SCFs and being the ideal choice for critical applications. In contrast, the chamfer shows a significant increase in SC compared to the shoulder by 80.4% under tension, 45.8% under torsion, and 76.3% under bending, making it an economical choice for non-critical applications. The key-seat demonstrates a varying behavior, achieving similar performance for the shoulder under tension (-2.6% difference), while recording the worst performance under torsion, increased by 101.6% from the shoulder. SCFs range from the lowest value of 1.197 for the shoulder fillet under torsion to the highest value of 2.967 under tension, underscoring the importance of choosing the right design depending on the type of expected load and operational safety requirements.

TABLE I. BENDING SCF AND ERROR PERCENTAGE BETWEEN ANALYTICAL AND NUMERICAL NOMINAL STRESS RESULTS

Case	1	2	3
Analytical nominal stress (MPa)	4.0764	4.0764	4.0764
FEA nominal stress (MPa)	4.0743	4.0743	4.0743
Error (%)	0.0515	0.0515	0.0515
FEA maximum shear stress (MPa)	5.8077	10.239	10.203
SCF K_{tB}	1.425	2.512	2.503

TABLE II. COMPARISON OF (SCFS) ACROSS ALL GEOMETRIES AND LOADING CONDITIONS

Loading condition	Tension	Torsion	Bending
Shoulder fillet SCF	1.645	1.197	1.425
Chamfer SCF	2.967	1.745	2.512
Key-seat SCF	1.603	2.413	2.503
Chamfer versus fillet (% increase)	80.40	45.80	76.30
Key-seat versus fillet (% increase)	-2.60	101.60	75.60
Chamfer versus key-seat (% difference)	85.10	-27.70	0.40

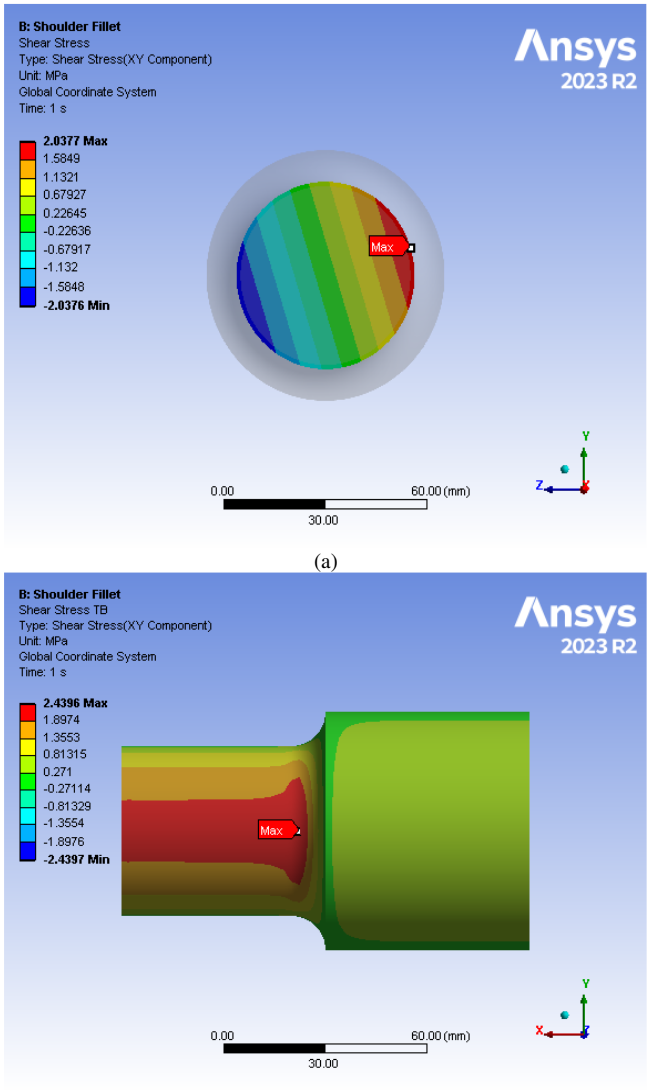

Fig. 12. Case 1 FEA results: (a) nominal shear stress, (b) maximum shear stress.

IV. CONCLUSIONS

The study presented a numerical analysis using ANSYS Workbench to analyze the shaft Stress concentration, which bridges the gap between academic Finite Element Analysis (FEA) and industrial shaft design by providing a validated tool for the Stress Concentration Factor (SCF) prediction. The findings demonstrate that the shoulder fillets (SCF=1.645) outperform chamfers under tension, while the key-seats require careful optimization under torsion. Compared to prior Finite Element Method (FEM) studies [7, 12], the proposed ANSYS framework offers a 15%-20% reduction in the computational time through optimized meshing strategies, making it suitable for iterative design workflows in automotive applications.

The main conclusions of this study are:

- The findings showed that in tension loads, SCF is nearly the same for the shaft shoulders and key-seat, and its value increased in the chamfer case.
- The results of the torsional loads revealed that the shoulder fillet case had the minimum SCF, while the maximum SCF was recorded in the key-seat case.
- The findings also demonstrated that the SCF values are almost the same for chamfer and key-seat cases when using bending loads, while the minimum SCF was observed in the shoulder fillet case.
- SCFs for the chamfers under tension (2.967) and torsion (1.745) exceeded fillets by 80% and 46%, respectively.
- The numerical analysis using ANSYS workbench provided nearly identical results compared to the analytical results, where the error percentage never exceeded 1%.
- The validation with previous studies has shown an error of less than 2%, confirming the reliability of the numerical approach.
- This study focused on static loads; dynamic or multiaxial loading analysis and experimental validation are proposed for future work.

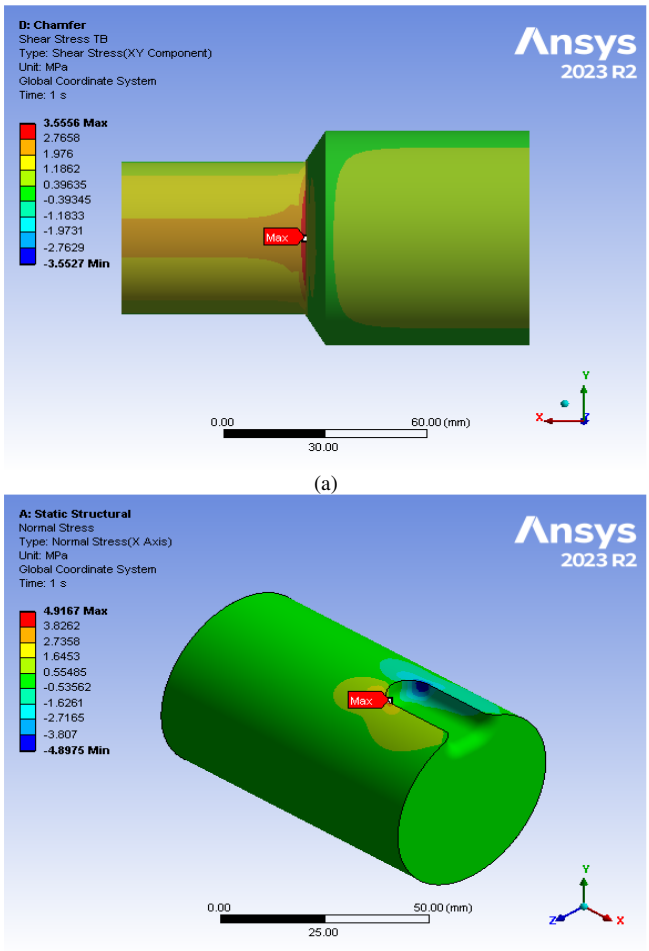

Fig. 13. FEA maximum shear stress: a) case 2, b) case 3.

REFERENCES

[1] W. D. Pilkey, D. F. Pilkey, and Z. Bi, Peterson, *Stress Concentration Factors*, 1st ed. Wiley, New Jersey, U.S., 2020.

[2] D. Y. Jang and J. H. Liou, "Study of stress development in axi-symmetric products processed by radial forging using a 3-D non-linear finite-element method," *Journal of Materials Processing Technology*, vol. 74, no. 1–3, pp. 74–82, Feb. 1998, https://doi.org/10.1016/s0924-0136(97)00252-5.

[3] A. N. Abbas Alani and A. H. Ali, "Investigating teeth root stresses of various spur gears using stress function and FEM," *Pollack Periodica*, vol. 18, no. 2, pp. 90–94, Jul. 2023, https://doi.org/10.1556/606.2022.00740.

[4] H. A. Musa and M. Q. Abdullah, "Influence of using Asymmetric Teeth Profile on Stress Concentrations in Gear Key-way," *IOP Conference Series: Materials Science and Engineering*, vol. 1094, no. 1, Feb. 2021, Art. no. 012067, https://doi.org/10.1088/1757-899x/1094/1/012067.

[5] M. Nuraliyev, M. A. Dundar, H. K. Akyildiz, and D. E. Sahin, "A novel approach for the determination of optimal diameter of shaft with keyway: Analytical and numerical study," *Mechanics Based Design of Structures and Machines*, vol. 52, no. 8, pp. 5610–5636, Aug. 2024, https://doi.org/10.1080/15397734.2023.2259968.

[6] N. L. Pedersen, "Optimal key design for shaft hub connections," in *Proceedings of the Institution of Mechanical Engineers, Part C: Journal of Mechanical Engineering Science*, vol. 238, no. 3, pp. 811–821, Feb. 2024, https://doi.org/10.1177/09544062231174125.

[7] P. B. N. De Assis, C. F. D. F. Moura Júnior, I. O. Andrade, W. N. Da Silva, and R. R. B. Medeiros, "Analysis of the influence of fillet geometry on stress concentration in keyway by the finite element method," *Observatório De La Economía Latinoamericana*, vol. 21, no. 11, pp. 22365–22375, Nov. 2023, https://doi.org/10.55905/oelv21n11-203.

[8] H R Prajapati, B P Patel, and N V Patel, "Investigation of Stress Concentration Factor for Keyway on Shaft under Different Loading Conditions: A Case Study." *University Journal of Research*, vol. 1, no. 1, 2015, https://doi.org/10.13140/RG.2.2.24744.67840.

[9] Faculty of Engineering, Beni-Suef University, Egypt and M. I. Sinossi, "Numerical Study of Gradual Change in Shaft Diameter and Relief Groove Radius on Stress Concentration Factor," *Eurasian Physical Technical Journal*, vol. 21, no. 3(49), pp. 125–131, Sep. 2024, https://doi.org/10.31489/2024no3/125-131.

[10] J. L. Do Vale and J. Da Silva, "Shape optimization applied in minimizing stress concentration factors: a case study for manufacturable shaft design," *Journal of the Brazilian Society of Mechanical Sciences and Engineering*, vol. 47, no. 2, Feb. 2025, https://doi.org/10.1007/s40430-024-05355-2.

[11] M. K. Sahu, and Pradeep, "Optimization of the Keyway Design with Consideration of Effect of Stress Concentration on Different Materials," *Engineering, Materials Science International journal of engineering research and technology*, vol. 2, no. 5, May. 2014.

[12] E. Izard, R. Garcia, M. Rodriguez-Martín, and M. Lorenzo, "Finite Element Analysis of the Reduction in Stress Concentration Factors in Shrink Fits by Using Contact Rings," *Applied Sciences*, vol. 12, no. 19, Oct. 2022, Art. no. 10037. https://doi.org/10.3390/app121910037.

[13] P. V Shanmukha, S. R. B. K. Krishna, K. K. B. Murali, R., T Lokesh Kumar, and K. S Vijay, "Stress Concentration Factors for Shouldered Shaft with Fillet and Taper Loaded in Tension," *International Journal of Scientific & Technology Research*, vol. 9, no. 04, Apr. 2020.

[14] M. T. Ozkan and F. Erdemir, "Determination of stress concentration factors for shafts under tension," *Materials Testing*, vol. 62, no. 4, pp. 413–421, Apr. 2020, https://doi.org/10.3139/120.111500.

[15] H. Adin, R. K. Ergün, and M. Ş. Adin, "Computer aided numerical damage analysis of the axle shaft," *European Mechanical Science*, vol. 6, no. 3, pp. 201–206, Sep. 2022, https://doi.org/10.26701/ems.1109917.

[16] M. T. Koçak and M. S. Bayraklilar, "Mechanical Shaft Optimization: a Study on Static Structural Analysis and Topological Optimization in Ansys," *International Journal of 3D Printing Technologies and Digital Industry*, vol. 7, no. 3, pp. 541–549, Dec. 2023, https://doi.org/10.46519/ij3dptdi.1366605.

[17] R. Kannojiya *et al*., "Performance Assessment of Stress Concentration Reduction Methods in Mild Steel Transmission Shaft," *International Journal of Engineering and Advanced Technology*, vol. 9, no. 3, pp. 4072–4076, Feb. 2020, https://doi.org/10.35940/ijeat.c5528.029320.

[18] A. Vijay, M. P. Vinayan, A. Hafsana, and T. Jagadeesha, "Design, Fatigue Analysis, and Optimization of Propeller Shafts Using Finite Element Analysis," in *Lecture Notes in Mechanical Engineering*, Singapore: Springer Nature Singapore, 2022, pp. 241–251.

[19] R. Raychev and I. Delova, "Methods for Reducing the Stress Concentration in Cylindrical Specimens, at Axial Loading," in *Proceedings of the International Scientific and Practical Conference*, vol. 3, pp. 300–303, Jun. 2021, https://doi.org/10.17770/etr2021vol3.6535.

[20] N. Rasovic, A. Cekic, and J. Kaljun, "Design and Simulation of the Controlled Failure of Custom-Built Rigid Shaft Coupling," *International Journal of Simulation Modelling*, vol. 21, no. 3, pp. 383–394, Sep. 2022, https://doi.org/10.2507/ijsimm21-3-596.

[21] E. Solangi, T. M. B. Albarody, S. Al-Challabi, J. A. Khan, and S. Ali, "Design and Failure Analysis of a Vacuum Pressure Vessel for Aerospace Applications using Finite Element Analysis (FEA)," *Engineering, Technology & Applied Science Research*, vol. 14, no. 6, pp. 17888–17893, Dec. 2024, https://doi.org/10.48084/etasr.7673.

[22] S. S. Patil, S. M. Patil, A. P. Bhattu, and A. D. Sahasrabudhe, "FEM Analysis and Optimization of Two Chamber Reactive Muffler by using Taguchi Method," *American International Journal of Research in Science, Technology, Engineering & Mathematics*, vol 1, no. 3, pp. 21–28, 2021.

[23] G. J. Matthews and C. J. Hooke, "Solution of axisymmetric torsion problems by point matching," *Journal of Strain Analysis*, vol. 6, no. 2, pp. 124–133, Apr. 1971, https://doi.org/10.1243/03093247v062124.